Asymmetric diffusion at the interfaces in Fe/Si multilayers

Ajay Gupta,* Dileep Kumar, and Vaishali Phatak
UGC-DAE Consortium for Scientific Research, University Campus, Khandwa Road, Indore 452017, India
(Received 30 December 2009; revised manuscript received 14 February 2010; published 1 April 2010)

Nanoscale diffusion at the interfaces in multilayers plays a vital role in controlling their physical properties for a variety of applications. In the present work depth-dependent interdiffusion in a Si/Fe/Si trilayer has been studied with subnanometer depth resolution using x-ray standing waves. High depth selectivity of the present technique allows one to measure diffusion at the two interfaces of Fe, namely, Fe on Si and Si on Fe independently, yielding an intriguing result that Fe diffusivity at the two interfaces is not symmetric. While the values of activation energy at the two interfaces are comparable, the main difference is found in the pre-exponent factor suggesting different mechanisms of diffusion at the two interfaces. This apparently counterintuitive result has been understood in terms of an asymmetric structure of the interfaces as revealed by depth selective conversion electron Mössbauer spectroscopy. This asymmetry is in turn explained by peculiarities during Si/Fe/Si layer formation by sputter deposition, in particular due to the difference between the surface free energies of Fe and Si.

DOI: 10.1103/PhysRevB.81.155402 PACS number(s): 68.65.Ac, 68.35.Fx, 68.49.Uv

Atomic diffusion is fundamental to many processes in materials science such as microstructure development, nonmartensitic phase transformation, stress relaxation, etc. In multilayers, atomic diffusion at the interfaces plays a vital role in controlling their physical properties for a wide variety of applications. In x-ray and neutron mirrors intentionally diffused interfaces have been used to reduce the higher order contamination.[1] In tunnel magnetoresistance multilayers, thermal annealing can increase magnetoresistance by orders of magnitude.[2] In giant magnetoresistance (GMR) multilayers, interdiffusion can significantly affect the GMR.[3] In spin valves with Mn based antiferromagnetic layer, Mn diffusion can seriously degrade the performance.[4] Co diffusion in Sm-Co/Fe exchange-spring magnet films is known to improve the exchange coupling.[5] While atomic diffusion in bulk solids is a widely studied and fairly well understood phenomenon, a reasonable understanding of the interfacial diffusion in multilayers has yet to emerge. Several factors such as a steep concentration gradient at the interfaces, interfacial stresses, and disorder may significantly modify the diffusion in multilayers. This has resulted in unexpected interfacial phenomenon such as a nonparabolic shift of phase boundaries in the presence of strong composition dependence of diffusivity.[6]

X-ray standing waves generated by total external reflection of x rays from buffer layer[7] or in a multilayer[8,9] have been used for concentration profiling of various elements. In the present work, we exploit the depth selectivity of x-ray standing waves for studying the depth-dependent interdiffusion in a Si/Fe/Si trilayer with subnanometer depth resolution. High depth sensitivity of the technique allows one to measure diffusion at the two interfaces of Fe, namely, Fe on Si and Si on Fe independently. It is found that diffusion at the Fe-on-Si interface is faster as compared to that on Si-on-Fe interface. In order to understand the possible origin of this asymmetry in diffusion, conversion electron Mössbauer spectroscopy (CEMS) has been used to study the interfacial structure. It is found that there is a significant difference in the structure of the two interfaces, which may be the cause of the asymmetry in the diffusivities at the two interfaces.

The structure of the multilayer used for diffusion measurements is $[\mathrm{W}\ (2.0\ \mathrm{nm})/\mathrm{Si}\ (3.1\ \mathrm{nm})]_{10}/\mathrm{Si}\ (3.8\ \mathrm{nm})/\mathrm{Fe}\ (2.7\ \mathrm{nm})/\mathrm{Si}\ (7.0\ \mathrm{nm})$ (referred as SW_ML). The deposition was done at room temperature using ion beam sputtering in a vacuum chamber with a base pressure of 1×10^{-7} mbar.[10] A broad beam Kaufman-type ion source was used with Ar ions with energy of 1 keV and a beam current of 20 mA. Ar gas pressure in the chamber during deposition was 2×10^{-4} mbar. The bottom $[\mathrm{W}\ (2.0\ \mathrm{nm})/\mathrm{Si}\ (3.1\ \mathrm{nm})]_{10}$ multilayer is used to generate x-ray standing waves.[9] On the top of this multilayer Si (3.8 nm)/Fe (2.7 nm)/Si (7.0 nm) structure was deposited without breaking vacuum. A thickness of 3.8 nm for the first Si layer is chosen in such a way that the Fe layer lies roughly midway between two antinodes of the x-ray standing waves generated in W/Si multilayer at the Bragg peak. This point is clear from Fig. 1 which shows the contour plot of x-ray intensity as a function of depth and the scattering vector q. At $q=1.35\ \mathrm{nm}^{-1}$ which corresponds to the center of the Bragg peak of W/Si multilayer, Fe layer is midway between the two antinodes.

Simultaneous x-ray reflectivity (XRR) and x-ray fluorescence measurements were done using Bruker D8 diffractometer fitted with a Göbble mirror on the incident beam side in order to obtain a parallel monochromatic beam of Cu $K\alpha$ radiation. Fluorescence spectrum was measured using a Ketek detector with an energy resolution of 200 eV. Thermal annealing of multilayer structure was done in a vacuum of 1×10^{-6} mbar in order to induce interdiffusion at the interfaces of Fe and Si layers. A separate study on the annealing behavior of W/Si multilayer showed that at least up to 623 K, the W/Si multilayer structure is stable with almost no change in its x-ray reflectivity. Thus the thermal annealing in the present multilayer essentially induces interdiffusion at the interfaces of Fe and Si layers only.

In order to study the Fe-on-Si and Si-on-Fe interfaces using CEMS, the following two multilayer structures were also prepared using ion beam sputtering: (i) substrate/$[\mathrm{Si}\ (6\ \mathrm{nm})/^{57}\mathrm{Fe}\ (2\ \mathrm{nm})/\mathrm{Fe}\ (2\ \mathrm{nm})]_{10}$ and (ii)

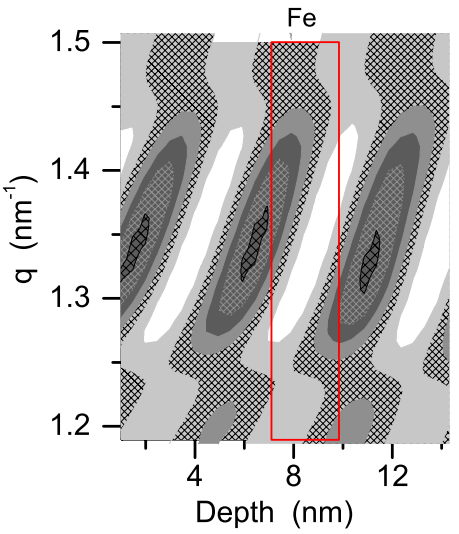

FIG. 1. (Color online) Contour plot of x-ray intensity as a function of q and depth from the surface of the multilayer. The rectangle represents the position of Fe layer.

substrate/[Si (6 nm)/Fe (2 nm)/^{57}Fe (2 nm)]$_{10}$, designed as ML1 and ML2, respectively. In the first multilayer the 2-nm-thick ^{57}Fe layer lies on Fe-on-Si interface, while in the second multilayer it lies on Si-on-Fe interface. Since Mössbauer measurements are sensitive only to ^{57}Fe, the first multilayer gives information preferentially about the Fe-on-Si interface, while the second one gives information about Si-on-Fe interface. The CEMS measurements were done using a Wissel Mössbauer spectrometer and a gas flow proportional counter with 95% He+5% CH_4.

SW_ML was isochronally annealed at 473, 498, 523, 598, and 623 K for 1 h each. Figure 2 gives some representative XRR of SW_ML after various stages of annealing. The XRR of this multilayer is dominated by that of W/Si multilayer mirror, with only small modulation in the q region below the

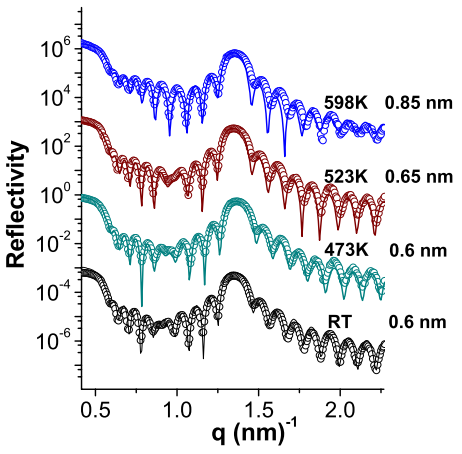

FIG. 2. (Color online) Representative XRR of SW_ML after various stages of annealing. The continuous curves represent the best fit to the experimental data. Different curves are displaced with respect to each other for easy viewing. The numbers shown against each curve represent annealing temperature and the average interface roughness of W/Si multilayer, respectively.

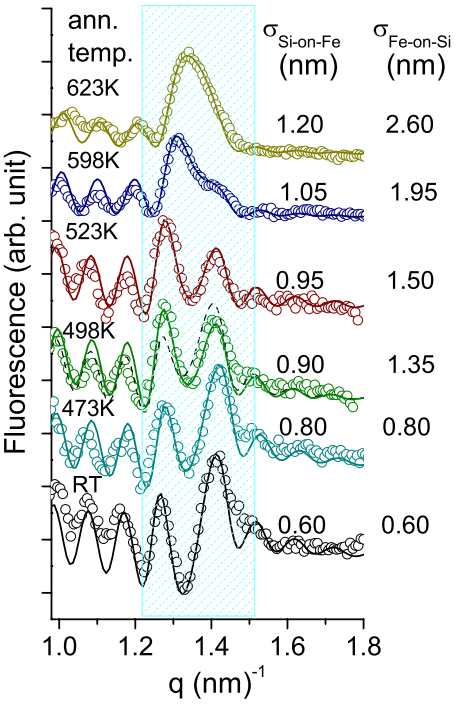

FIG. 3. (Color online) Fe fluorescence of SW_ML after various stages of annealing. The continuous curves represent the best fit to the experimental data. The shaded area represents the region around Bragg peak where x-ray standing waves are formed. The dashed curve represents the best fit to the experimental data of 498 K annealed sample with the roughnesses of the two interfaces of Fe taken to be equal.

Bragg peak attributable to the top Si/Fe/Si trilayer. Figure 3 shows Fe-fluorescence data of SW_ML measured simultaneously with XRR. The region around the Bragg peak in which x-ray standing waves are generated is highlighted in the figure by shaded area. One may note that in the as-deposited sample Fe fluorescence exhibits two well-defined peaks in the region where x-ray standing waves are generated. The origin of these two peaks can be understood from the contour plot of x-ray intensity (Fig. 1). At the center of the Bragg peak, Fe layer lies roughly midway between the two antinodes. However, as one moves away on either side of the Bragg peak, the antinodes get shifted resulting in partial overlapping of one of the antinodes with Fe layer, giving rise to a peak in Fe fluorescence. The peak around $q = 1.27$ nm^{-1} corresponds to a situation where one of the antinodes partially overlaps with Fe-on-Si interface, while the peak at $q = 1.41$ nm^{-1} occurs as a result of partial overlap of an antinode at Si-on-Fe interface. With thermal annealing both these peaks get broadened and their intensities get modified. However, changes occurring in the two peaks are quite different, suggesting that the two interfaces get modified differently with thermal annealing. Simultaneous fitting of XRR and Fe-fluorescence data has been done using Parratts formalism.[11] For the pristine sample, fittings were done by taking average thicknesses and interface roughnesses of W and Si layers of the W/Si standing wave generator, as well as the thicknesses and interface/surface roughnesses of Si and Fe layers as variable parameters. In addition, it was

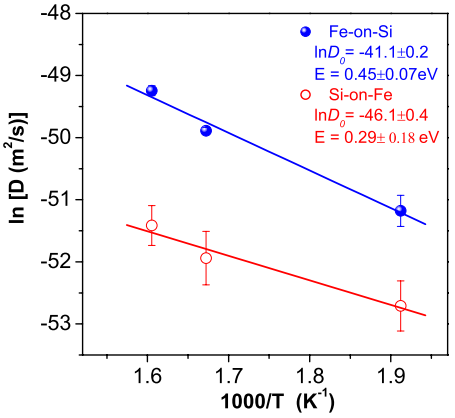

FIG. 4. (Color online) Arrhenius plot of Fe diffusivity at the two interfaces.

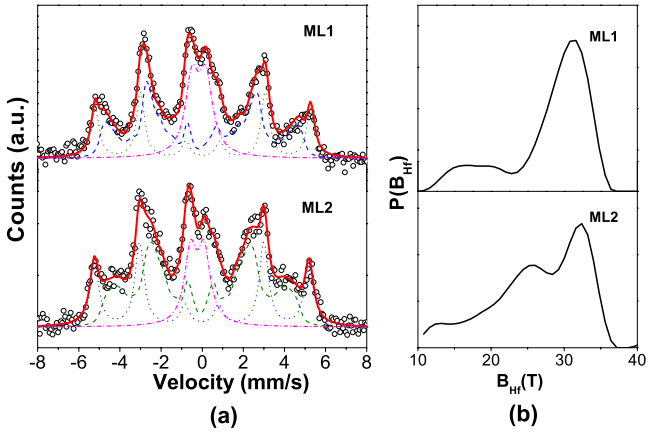

FIG. 5. (Color online) (a) Conversion electron Mössbauer spectra of as-deposited ML1 and ML2. (b) The corresponding hyperfine field distribution of the broad magnetic sextet.

found necessary to take a silicon oxide layer of 3 nm thickness at the surface with an electron density of 10% less than that of Si layer. Only marginal variations in the layer thicknesses from the nominal values were observed. For the subsequently annealed sample, only roughnesses were varied, while the layer thicknesses were kept constant at the values obtained from the fitting of the pristine sample. This is consistent with the fact that the same piece of the sample was successively annealed at different temperatures. While the XRR data are mainly sensitive to the changes in $\sigma_{W/Si}$, the Fe fluorescence is affected by the changes in the structure of the interfaces of Fe layer. Thus, a simultaneous fitting of both reflectivity and fluorescence data gives a reliable estimation of various parameters. One finds that with thermal annealing up to 623 K, there are only minor changes in the W/Si multilayer with the interface roughness going from 0.6 to 0.85 nm, while the roughnesses of the two interfaces of Fe increase substantially with thermal annealing. One may note that the roughness of Fe-on-Si interface increases at a much faster rate as compared to that of Si-on-Fe interface. It may be mentioned that for the thermal annealing up to 473 K, the width of Fe concentration profile is much smaller than the separation between two antinodes. Therefore, from the fluorescence data it is difficult to estimate the roughnesses of the two interfaces separately. However, at 498 K and above roughnesses of the two interfaces can be determined individually with good reliability. In order to demonstrate this point, the fitting of 498 K data obtained by taking the roughnesses of the two interfaces to be equal is also shown in Fig. 3 (dashed curve). The best fitted curve with such a constraint clearly deviates from the experimental data.

The variation in the roughnesses of the two interfaces with the thermal annealing has been used to estimate the diffusivity of Fe at the two interfaces using the relation[12]

$$D(T_i) = [\sigma^2(T_i) - \sigma^2(T_{i-1})]/2t, \tag{1}$$

where $D(T_i)$ is the diffusion coefficient at temperature T_i and $\sigma(T_{i-1})$ and $\sigma(T_i)$ are the roughnesses of an interface before and after annealing at temperature T_i for time t. Figure 4 gives the Arrhenius plot of ln D versus $1/T$ at the two interfaces of Fe. One finds that there is a significant difference in Fe diffusivities at the two interfaces. A linear fit to the experimental data as expected from the Arrhenius temperature dependence of the diffusivity,

$$D(T) = D_0 \exp(-E/K_B T), \tag{2}$$

yields the activation energy E as well as the pre-exponent D_0 for the diffusion. The experimentally obtained values are shown in Fig. 4. One finds that the activation energies for diffusion at the two interfaces are comparable within experimental errors. However, the pre-exponent D_0 is significantly high for Fe-on-Si interface as compared to that for Si-on-Fe interface, resulting in a significantly high diffusivity at Fe-on-Si interface in the temperature range studied in the present experiment.

At first glance, the above results appear to be counterintuitive as both interfaces ought to be identical, having Fe layer on one side and Si layers on the other. In order to understand the possible reason for this difference in the diffusivity at the two interfaces, a detailed study of the structure of the two interfaces has been done using CEMS on samples ML1 and ML2. As discussed in the experimental section CEMS of ML1 is sensitive to Fe-on-Si interface while that of ML2 is sensitive to Si-on-Fe interface.

Figure 5(a) shows Mössbauer spectra of ML1 and ML2 in as-deposited state. The spectra of both the specimens are fitted with three overlapping components: (1) a sharp sextet with hyperfine field of about 33 T, (2) a broad magnetic component, having a distribution of hyperfine fields, and (3) a nonmagnetic doublet. The sharp sextet represents the bulk of α-Fe, while the broad magnetic component and the doublet represent the Fe atoms in the interfacial region. Further it is known that in Fe-Si alloy, if iron concentration is less than 50%, it becomes nonmagnetic.[13] Therefore, the area under the doublet represents the fraction of Fe atoms in the interfacial region having iron concentration less than or equal to 50%. Results of fitting are given in Table I. One may note that the area under the sharp sextet in both the specimens is about 30% within experimental errors. However, the relative areas of broad magnetic component and the doublet as well as the shape of the hyperfine field distribution of

TABLE I. Results of fitting of Mössbauer spectra of ML1 and ML2 as described in the text. δ, Δ, and B_{hf} represent isomer shift, quadrupole splitting, and average hyperfine field, respectively. Isomer shift δ is with respect to α-Fe.

Sample		ML1	ML2
Sharp sextet	$B_{hf}(T)$	31.34 ± 0.08	32.32 ± 0.06
	Area (%)	28 ± 6	32 ± 5
Broad sextet	$B_{hf}(T)$	26.11 ± 0.32	25.74 ± 0.21
	Area (%)	46 ± 6	50 ± 3
Doublet	δ (mm/s)	0.16 ± 0.01	0.24 ± 0.01
	Δ (mm/s)	0.68 ± 0.02	0.65 ± 0.03
	Area (%)	26 ± 3	18 ± 3

broad magnetic component [Fig. 5(b)] are very different in the two specimens. This suggests that the structure of the two interfaces, namely, Si-on-Fe and Fe-on-Si interfaces, may be different. A rough estimate of the interface roughness as obtained from the width of the intermixed region comes out to be 0.78 nm, which is in agreement with that obtained from x-ray measurements. From Table I, one finds that at Si-on-Fe interface, the fraction of Fe atoms in the doublet is 18%, which is 26% of the total Fe atoms in the intermixed region. This area fraction agrees very well with that expected for an error function concentration profile [Fig. 6]. Thus, Mössbauer measurements suggest that the concentration profile at Si-on-Fe interface is an error function.

From Mössbauer spectrum of specimen ML1 one finds that in this spectrum, the area of doublet is 26%, which is significantly more than what one expects for an error function concentration profile. Further a comparison of hyperfine field distributions at the two interfaces [Fig. 5(b)] shows that at Si-on-Fe interface, there is a continuous distribution of hyperfine field values starting from 32 down to 10 T while at Fe-on-Si interface, low field components are missing. The above two differences can be understood if one assumes the concentration profile at Fe-on-Si interface, as shown schematically in Fig. 6, where the area from the low field magnetic component gets transferred to the nonmagnetic component. This suggests that at Fe-on-Si interface, there is an interlayer of $Fe_{1-x}Si_x$, resulting in a plateau in the concentration profile. The isomer shift and quadrupole values of the doublet of ML1 match very well with those of $FeSi_2$, suggesting that the composition of interlayer is $FeSi_2$.[14] This result is in agreement with some earlier works on the same system.[15,16] Thus, at Fe-on-Si interface diffusion occurs via the $FeSi_2$ interlayer, while at Si-on-Fe interface diffusion occurs via bcc Fe with some Si dissolved in it. In literature the diffusivity data for self-diffusion in stoichometric Fe_3Si phase as well as intermetallic compounds of FeSi are given. However, it is not meaningful to compare the diffusivities obtained in the present work at the two interfaces with bulk diffusivities since it is known that the multilayer diffusivities

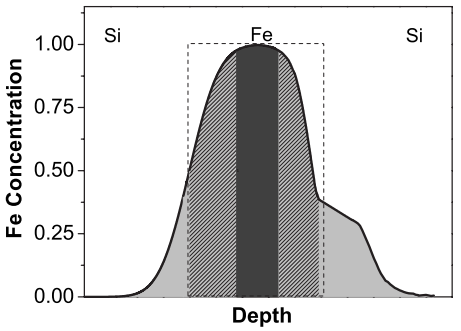

FIG. 6. Schematic diagram of concentration profile of Fe layer. The Si-on-Fe interface has an error function profile, while at Fe-on-Si interface, there is a plateau region corresponding to $FeSi_2$ phase. The regions corresponding to sharp sextet, broad sextet, and doublet are shown in different shades. The dashed rectangle shows the position of ideal interfaces.

at the interfaces are very different because of high concentration of defects and possible concentration gradient.[17]

The difference in the structure of the two interfaces can be understood in terms of the difference in the surface free energies of Fe (2.9 J m^{-2}) and Si (1.2 J m^{-2}).[18] During the deposition of Fe on Si, the surface free energy of Si being lower, Si atoms try to move to the surface guided by the chemical driving force. This would lead to a stronger mixing at the interface and a possible formation of $FeSi_2$ compound. On the other hand, during the deposition of Si on Fe, no such chemical driving force exists; therefore the intermixing at Si-on-Fe interface would take place as a result of random thermal motions only and hence concentration profile is expected to be an error function.

In conclusion, x-ray standing wave technique has been used to get concentration profile of Fe layer in Si/Fe/Si trilayer. The precision of this technique is sufficiently high to differentiate between the two interfaces of the Fe layer. This allows one to study interdiffusion at the two interfaces, namely, Fe on Si and Si on Fe independently. Interestingly the diffusivities at the two interfaces are significantly different. This seemingly counterintuitive result can be understood in terms of a difference in the structure of the two interfaces in the as-deposited film itself. CEMS measurements show that while at Si-on-Fe interface the Fe concentration profile is an error function, at Fe-on-Si interface an interlayer exists with approximate composition of $FeSi_2$. This difference in the structure of the two interfaces is the cause of different diffusivities at the two interfaces. Besides being of fundamental importance in understanding the interfacial diffusion at nanometer scale, present results have important implications on the use of controlled thermal annealing for tailoring the properties of multilayers for a wide variety of applications.

Partial support from the Indo-French Center for Promotion of Advanced Research is acknowledged.

*agupta@csr.ernet.in

[1] J. Padiyath, J. Stahn, M. Horisberger, and P. Böni, Appl. Phys. Lett. **89**, 113123 (2006).
[2] J. Scola, H. Polovy, C. Fermon, M. Pannetier-Lecoeur, G. Feng, K. Fahy, and J. M. D. Coey, Appl. Phys. Lett. **90**, 252501 (2007).
[3] D. Iuşan, M. Alouani, O. Bengone, and O. Eriksson, Phys. Rev. B **75**, 024412 (2007).
[4] S. H. Jang, T. Kang, H. J. Kim, and K. Y. Kim, Appl. Phys. Lett. **81**, 105 (2002).
[5] Y. Choi *et al.*, Phys. Rev. B **75**, 104432 (2007).
[6] Z. Erdélyi, M. Sladecek, L.-M. Stadler, I. Zizak, G. A. Langer, M. Kis-Varga, D. L. Beke, and B. Sepiol, Science **306**, 1913 (2004).
[7] A. Gupta, P. Rajput, A. Saraiya, V. R. Reddy, M. Gupta, S. Bernstorff, and H. Amenitsch, Phys. Rev. B **72**, 075436 (2005).
[8] M. J. Bedzyk, G. M. Bommarito, M. Caffrey, and T. L. Penner, Science **248**, 52 (1990).
[9] A. Gupta, D. Kumar, and C. Meneghini, Phys. Rev. B **75**, 064424 (2007).
[10] M. Gupta, A. Gupta, D. M. Phase, S. M. Chaudhari, and B. A. Dassanacharya, Appl. Surf. Sci. **205**, 309 (2003).
[11] L. G. Parratt, Phys. Rev. **95**, 359 (1954).
[12] H. Mehrer, *Atomic Diffusion in Solids: Fundamentals, Methods, Materials, Diffusion-Controlled Processes* (Springer, Berlin, 2007).
[13] M. Walterfang, W. Keune, K. Trounov, R. Peters, U. Rucker, and K. Westerholt, Phys. Rev. B **73**, 214423 (2006).
[14] J. Desimoni, F. H. Sanchez, M. B. Fernandez van Raap, X. W. Lin, H. Bernas, and C. Clerc, Phys. Rev. B **54**, 12787 (1996).
[15] E. V. Chubunova, I. Khabelashvili, Y. Y. Lebedinskii, V. N. Nevolin, and A. Zenkevich, Thin Solid Films **247**, 39 (1994).
[16] G. J. Strijkers, J. T. Kohlhepp, H. J. M. Swagten, and W. J. M. de Jonge, Phys. Rev. B **60**, 9583 (1999).
[17] W. H. Wang, H. Y. Bai, M. Zhang, J. H. Zhao, X. Y. Zhang, and W. K. Wang, Phys. Rev. B **59**, 10811 (1999).
[18] F. J. Himpsel, J. E. Ortega, G. J. Mankey, and R. F. Willis, Adv. Phys. **47**, 511 (1998).